A&A 564, A24 (2014)
DOI: 10.1051/0004-6361/201323163

Astronomy & Astrophysics

Calculations with spectroscopic accuracy: energies, transition rates, and Landé g_J-factors in the carbon isoelectronic sequence from Ar XIII to Zn XXV⋆,⋆⋆

J. Ekman[1], P. Jönsson[1], S. Gustafsson[1], H. Hartman[1], G. Gaigalas[2], M.R. Godefroid[3], and C. Froese Fischer[4]

[1] Materials Science and Applied Mathematics, Malmö University, 21120 Malmö, Sweden
e-mail: jorgen.ekman@mah.se
[2] Vilnius University, Institute of Theoretical Physics and Astronomy, A. Goštauto 12, 01108, Vilnius, Lithuania
[3] Chimie Quantique et Photophysique, CP160/09, Université Libre de Bruxelles, Av. F.D. Roosevelt 50, 1050 Brussels, Belgium
[4] Department of Electrical Engineering and Computer Science, Box 1679B, Vanderbilt University, TN 37235, USA

Received 1 December 2013 / Accepted 5 February 2014

ABSTRACT

Extensive self-consistent multiconfiguration Dirac-Hartree-Fock (MCDHF) calculations and subsequent relativistic configuration interaction calculations are performed for 262 states belonging to the 15 configurations $2s^22p^2$, $2s2p^3$, $2p^4$, $2s^22p3l$, $2s2p^23l$, $2p^33l$ and $2s^22p4l$ ($l = 0, 1, 2$) in selected carbon-like ions from Ar XIII to Zn XXV. Electron correlation effects are accounted for through large configuration state function expansions. Calculated energy levels are compared with existing theoretical calculations and data from the Chianti and NIST databases. In addition, Landé g_J-factors and radiative electric dipole transition rates are given for all ions. The accuracy of the calculations are high enough to facilitate the identification of observed spectral lines.

Key words. atomic data

1. Introduction

The observation of emission lines from carbon-like ions in spectra consitutes an important tool for diagnostics of astrophysical and fusion plasmas. For instance, lines in Fe XXI are strong candidates for spectral diagnostics of solar flares observed with the Solar Dynamics Obervatory (Del Zanna et al. 2013) where the transitions between the lowest configurations, $2s^22p^2$ and $2s2p^3$, are found in the wavelength region 100−150 Å. Ratios of these lines are used as density probes. Depending on the plasma density and the blending lines from other species in the spectrum of the source studied, different lines must be used. Transitions between the $2s^22p^2$ and $2s^22p3d$ configurations appear in the region around 12 Å. These lines are closely spaced, and higher resolution observations are required to avoid blended lines. On the other hand, the line ratios are less sensitive to instrumental response. A third group of lines are the M1 transitions within the ground configuration, $2s^22p^2$, with terms ^{3}P, ^{1}D, and ^{1}S. The transitions within the ^{3}P term appear at 1380 Å and 2295 Å, whereas lines from the singlet levels have shorter wavelengths, 300−800 Å. The triplet lines are excellent for electron density, n_e, diagnostics in the range 10^{11}−10^{13} cm^{-3}, typical solar flare conditions. The singlet levels reach Boltzmann equilibrium at higher densities and the corresponding lines can be used for densities up to 10^{15} cm^{-3}. The lines are thus ideal for tokamak conditions (Mason et al. 1979).

To interpret observed spectra, knowledge of accurate transition parameters such as transition rates is necessary. Previously a plethora of theoretical calculations and a few experimental studies on carbon-like systems have been made. A lot of work has been devoted to describe autoionization states in the isoelectronic sequence. Using the HFR (Cowan 1981) and AUTOSTRUCTURE (Eissner et al. 1974; Badnell 1986, 1997) atomic structure codes, Palmeri et al. (2008) reported calculations on K-vacancy level energies and transition rates for carbon-like Ne, Mg, Si, S, Ar and Ca ions. Autoionization- and radiative transition rates for carbon-like ions with $6 \le Z \le 54$ have been calculated by Safronova et al. (1999) using the $1/Z$ pertubation theory method and by Chen et al. (1997) with the multiconfiguration Dirac-Hartree-Fock (MCDHF) approach. Other publications report on transition and energy level data below the first ionization limit. For example, oscillator strengths have been calculated for transions between F IV and Ar XIII and between Ar XIII and Mn XX (Aggarwal et al. 2001, 2003, 2005). Transition energies and probabilities for Ar XIII from MCDHF calculations have been reported by Costa et al. (2001). Calculated energy levels and oscillator strengths in Ti XVII and Ni XXIII have been reported in Hu et al. (2011a) and Hu et al. (2011b), respectively. In addition, intercombination transitions for a wide range of ions in the C-like sequence between the $2s^22p^2\ ^3P_{1,2}$ and $2s2p^3\ ^5S^\circ_2$ levels have been calculated by Liu et al. (2013) and observed spin-forbidden lines in the 500−1600 Å range emitted by solar coronal plasmas have been compiled and improved energy levels have been deduced by Feldman et al. (2007). However, the extensive calculations on $2l \rightarrow 3l'$ transitions in L-shell Fe and Ni ions by Gu (2005a)

⋆ Research supported in part by the Swedish Research council, Swedish Institute and by the IUAP-Belgian State Science Policy (BriX network P7/12).

⋆⋆ Tables of energy levels and transition rates (Tables 3−22) are only available at the CDS via anonymous ftp to cdsarc.u-strasbg.fr (130.79.128.5) or via http://cdsarc.u-strasbg.fr/viz-bin/qcat?J/A+A/564/A24

are so far the most accurate reported in the sequence, when compared with observed level energies. In these calculations a combined configuration interaction and relativistic many-body pertubation theory (RMBPT) approach was used. Later work by the same author has been extended to include higher-n energies and transitions (Gu 2005b, 2007).

The present work aims at improving and extending the calculations by Gu, providing data of spectroscopic accuracy for a number of ions in the carbon-like sequence. In this context spectroscopic accuracy is related to the notion of calculated transition energies that are accurate enough to directly confirm or revise experimental identifications. In addition, the calculations also serve as benchmarks for other theoretical works (Jönsson et al. 2013b).

2. Multiconfiguration Dirac-Hartree-Fock

In the relativistic MCDHF method a natural starting point is the Dirac-Coloumb Hamiltonian. Using Hartree atomic units and subtracting the electron rest mass the latter is given by

$$H_{\rm DC} = \sum_{i=1}^{N}\left(c\,\boldsymbol{\alpha}_i\cdot\boldsymbol{p}_i + (\beta_i-1)c^2 + V_i\right) + \sum_{i>j}^{N}\frac{1}{r_{ij}}, \tag{1}$$

where V_i is the monopole part of the electron-nucleus interaction, r_{ij} the distance between electrons i and j, and $\boldsymbol{\alpha}$ and β are the Dirac matrices. The atomic state functions $\Psi(\gamma PJ)$ are expanded in terms of configuration state functions (CSFs), $\Phi(\gamma_j PJ)$, with appropriate J symmetry and parity P, namely

$$\Psi(\gamma PJ) = \sum_{j=1}^{M} c_j\Phi(\gamma_j PJ), \tag{2}$$

where γ_j represents the configuration and other quantum numbers needed to uniquely specify the state j. The CSFs are built from products of one-electron Dirac orbitals. The radial parts of the latter and the expansion coefficients c_j of the multiconfiguration expansion (2) are obtained in the relativistic self-consistent field (RSCF) procedure (Grant 2007). The Breit interaction

$$H_{\rm Breit} = -\sum_{i<j}^{N}\left[\boldsymbol{\alpha}_i\cdot\boldsymbol{\alpha}_j\frac{\cos(\omega_{ij}r_{ij}/c)}{r_{ij}} + (\boldsymbol{\alpha}_i\cdot\boldsymbol{\nabla}_i)(\boldsymbol{\alpha}_j\cdot\boldsymbol{\nabla}_j)\frac{\cos(\omega_{ij}r_{ij}/c)-1}{\omega_{ij}^2 r_{ij}/c^2}\right] \tag{3}$$

as well as leading quantum electrodynamic (QED) corrections can be included in subsequent relativistic configuration interaction (RCI) calculations (McKenzie et al. 1980). Calculations can be done for single levels, but also for portions of a spectrum in the extended optimal level (EOL) scheme, where optimization is applied on a weighted sum of energies (Dyall et al. 1989). All calculations were performed with a new release (Jönsson et al. 2013a) of the GRASP2K code (Jönsson et al. 2007).

3. Computation of Landé g_J-factors and transition parameters

Given a set of atomic state functions, measurable properties whose operators are expressed in tensor form, $\mathbf{T}^{(k)}$, can be obtained as reduced matrix elements,

$$\langle\,\gamma PJ\,\|\mathbf{T}^{(k)}\|\,\gamma' P' J'\,\rangle, \tag{4}$$

which, after inserting the CSF expansions, reduce to a sum over matrix elements between CSFs. Using Racah algebra techniques these matrix elements are finally obtained as sums over radial integrals (Gaigalas et al. 2001).

3.1. Landé g_J-factors

Under the influence of an external magnetic field, the Landé g_J-factors describe the first-order magnitude of the splitting of atomic levels into magnetic sub-levels of an atom (or ion). Moreover they provide information about the coupling in the system (Froese Fischer & Jönsson 2001). The g_J-factors are given by

$$g_J = \frac{2}{\sqrt{J(J+1)}} \times\left\langle\gamma PJ\left\|\sum_{j=1}^{N}\left[-\mathrm{i}\frac{c^2}{\sqrt{2}}\,r_j\left(\boldsymbol{\alpha}_j\,\mathbf{C}^{(1)}(j)\right)^{(1)} + \frac{g_s-2}{2}\beta_j\boldsymbol{\Sigma}_j\right]\right\|\gamma PJ\right\rangle, \tag{5}$$

where $\mathrm{i}=\sqrt{-1}$ is the imaginary unit, $\boldsymbol{\Sigma}_j$ is the relativistic spin-matrix and $g_{\rm s}=2.00232$ is the QED-corrected g-factor of the electron spin. The g_J-factors were calculated using the Zeeman module of GRASP2K (Andersson & Jönsson 2008).

In the context of astrophysics it should be pointed out that strong magnetic fields have been detected in hot [O, B, and A] stars (Petit 2011). The magnetic field strength is of the order of several tens of kG. The study of these magnetic fields in stars requires accurate Landé g_J-factors.

3.2. Transition parameters

The transition rates for electric dipole transitions between atomic states γPJ and $\gamma' P' J'$ can be expressed in terms of reduced matrix elements

$$\left\langle\gamma PJ\|\mathbf{D}^{(1)}\|\gamma' P' J'\right\rangle, \tag{6}$$

where $\mathbf{D}^{(1)}$ is the electromagnetic dipole operator in length (Babushkin) or velocity (Coulomb) gauge (Grant 1974). Using standard techniques the reduced matrix elements can be derived under the assumption that the atomic state functions are built from the same orthogonal radial orbital set (Gaigalas et al. 2001). However, this restriction can be relaxed and when two atomic state functions are described by independently optimized orbital sets, transformations of the atomic state functions are performed in such a way that the orbital sets become biorthogonal, in which case the calculation can proceed using standard Racah algebra (Olsen et al. 1995; Jönsson & Froese Fischer 1998).

4. Calculations

The 7 even parity $2s^22p^2$, $2p^4$, $2s^22p3p$, $2s2p^23s$, $2s2p^23d$, $2p^33p$ and $2s^22p4p$ configurations and the 8 odd parity $2s2p^3$, $2s^22p3s$, $2s^22p3d$, $2s2p^23p$, $2p^33s$, $2p^33d$, $2s^22p4s$ and $2s^22p4d$ configurations were chosen as reference configurations. Two MCDHF calculations in the EOL scheme were performed as a starting point: one calculation describing the 130 even parity levels and another the 132 odd parity levels with CSFs obtained from single- and double- (SD) excitations from all occupied orbitals of the odd and even parity reference configurations, respectively, to active sets {4s3p2d} (4 s-orbitals, 3 p-orbitals,

and 2 d-orbitals). To account for electron correlation these calculations were followed by a series of calculations where the active sets were consecutively enlarged, layer by layer, by adding one orbital for each l up to {9s8p7d5f5g3h}. For the last three layers, the SD excitations from the outer orbitals of the reference configurations were included, keeping $1s$ orbital closed. In the process the calculated properties were carefully monitored to ensure that a satisfactory convergence was obtained. These calculations were followed by final RCI calculations, one for each parity, where SD excitations were allowed from all orbitals of the reference configurations to the largest active sets {9s8p7d5f5g3h} and with QED- and Breit contributions taken into account. The resulting expansions consisted of 1 633 000 and 1 703 000 CSFs distributed over the $J = 0, 1, ..., 5$ angular symmetries for even and odd parity, respectively.

4.1. Labeling of states

The wave functions are given as expansions over jj-coupled CSFs. However, in the jj-coupling scheme the states are often not well described and in the expansions, many CSFs may have nearly the same weight. In this work we used a module in the latest release of the GRASP2K code (Jönsson et al. 2013a) to transform from jj- to LS-coupling and to obtain the leading LS-percentage composition. In general, this gives a good consistency with the labeling system used by the experimentalists as well as with the NIST database and other sources. It should be noted that also in LS-coupling, although to a less extent, different states sometimes share the same configuration and shell-coupling, as the leading component in the LS-percentage eigenvector composition. For these states an extended, but still truncated, composition can be used as the label.

5. Results and discussion

Figure 1 shows the gross structure of the calculated energy levels for ions in the carbon isoelectronic sequence. It is seen that the energy levels are clearly divided in two parts. The lower part consists of levels originating from the even parity $2s^22p^2$ and $2p^4$ configurations and the odd parity $2s2p^3$ configuration whereas the upper part consists of configurations of both parities that include one electron in either the $n = 3$ or $n = 4$ shell.

In terms of experimental work and accurate calculations, Fe XXI is currently the most studied ion in the carbon isoelectronic sequence so far. Therefore results from the present calculations are validated against experimental data and other theoretical predictions for this system. In Table 1 level energies for Fe XXI from calculations in this work are compared with calculated energies from a previous MCDHF/RCI calculation (RCI2) by Jönsson et al. (2011), relativistic many-body pertubation theory (RMBPT) by Gu (2005a) and from a calculation using the Flexible Atomic Code (FAC) by Landi & Gu (2006). Collected in Table 1 are also observed experimental level energies from NIST (NIST Atomic Spectra Database 2013) and Chianti (Landi et al. 2012) databases. Observed levels from the NIST database are from Sugar & Corliss (1985) and observed levels from the Chianti database are from Feldman et al. (2000); Martin et al. (1999); Brown et al. (2002); Landi & Phillips (2005). Whereas there is an excellent general agreement for the lower part (levels 1−20) between present calculations, calculations by Jönsson et al. (2011), Gu (2005a), and experimental data it is seen that Landi & Gu (2006) overestimated excitation energies significantly. These observations are manifested in

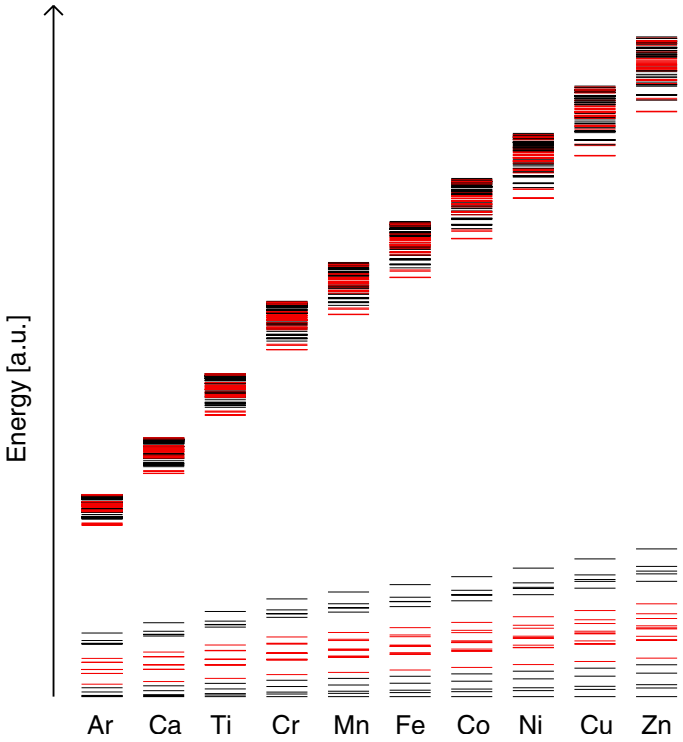

Fig. 1. Gross structure of calculated energy levels in the carbon isoelectronic sequence. Levels for odd parity states are colored red whereas levels for even parity states are displayed in black. Level energies are shown to scale, but given in arbitrary units.

a mean relative energy difference between calculations and observations of 0.028%–0.032% for this work, 0.023%–0.027% for RCI2, 0.035%–0.038% for RMBPT and 0.641%–0.646% for FAC, where lower (higher) values refer to experimental data from NIST (Chianti) databases. To quantify shifted absolute energy differences the mean level devation (MLD) according to

$$MLD = \frac{1}{N}\sum_{i=1}^{N} |E_{\rm obs}(i) - E_{\rm calc}(i) + ES|, \quad (7)$$

was used. The energy shift (ES) is chosen as to minimize the sum and indicates to what extent the ground state level is favored (ES positive) or unfavored (ES negative) in the theoretical binding energy balance. The obtained MLD (ES) values for level 1−20 are 137 (130) cm^{-1} for this work, 141 (100) cm^{-1} for RCI2, 175 (215) cm^{-1} for RMBPT and 5017 (3800) cm^{-1} for FAC, where recommended NIST values where used as $E_{\rm obs}$. Going beyond level 20 experimental observations are more scarce and the identification of levels becomes problematic in some cases. For example, the $2s^22p3d\ ^1D^\circ_2$ (8 098 000 cm^{-1}), $2s^22p3d\ ^3D^\circ_2$ (8 187 400 cm^{-1}) and $2s^22p4d\ ^3P^\circ_2$ (10 548 000 cm^{-1}) levels in the NIST database do not have any obvious counterparts in calculated energies or in the Chianti database. In addition, the $2s^22p3d\ ^3D^\circ_3$ (8 195 000 cm^{-1}) level (Sugar & Corliss 1985) from the NIST database is observed at a considerably lower energy (>30 000 cm^{-1}) than in other sources and a misidentification cannot be ruled out. The agreement with observed energies from the Chianti database is better. In two cases (level 37 and 75) the leading LS terms in this work do not agree with the LS terms given in the Chianti database. However, for these levels significant term mixing is present and taking into account the second largest contribution in the LS-composition (see Table 9 at the CDS), identification is possible. Comparing with experimental

data from the Chianti database, mean relative energy differences above level 20 are 0.050% for this work, 0.058% for RMBPT and 0.076% for FAC. A closer inspection of Table 1 reveals that the RMBPT energies above level 20 are on average predicted 800 cm^{-1} above the energies from the RCI calculation. RMBPT level energies in the lower part, below level 21, are also overpredicted, but to a less extent. The same observation was made in Jönsson et al. (2013b), where spectroscopic calculations were performed on boron-like Si using the same method as in the present work and compared with results from RMBPT calculations. All together it is fair to argue that the present RCI level energies reach spectroscopic accuracy and that the accuracy is better than for RMBPT calculated energies.

The material at the CDS also contain Landé g_J factors for all levels and ions considered. It is wortwhile to point out that in the presence of strong LS-mixing, the g_J factors differ substantially from what is obtained in the LS-coupling scheme. For example, the g_J-value obtained in this work for the highly mixed $2s^2 2p3p\ ^3P_1$:2 level in Fe XXI (level 29 in Table 9) is a factor of 2 larger than the corresponding value in the LS-scheme.

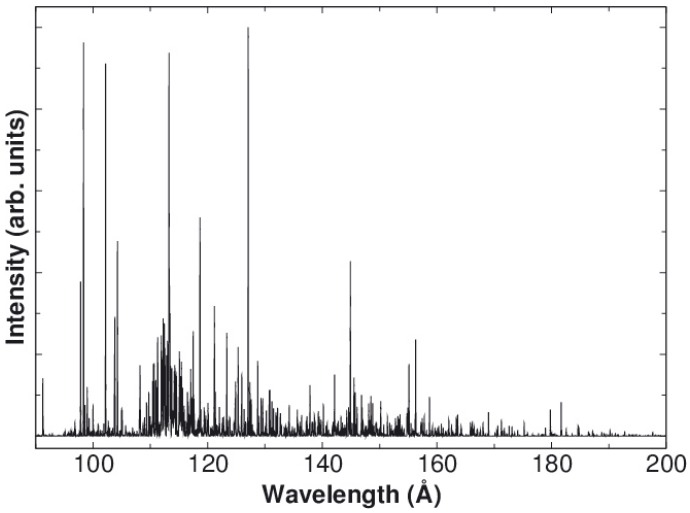

Fig. 2. Synthetic Fe XXI spectrum containing transitions between 90−200 Å from the present calculation. See text for details.

5.1. Transition rates

In Table 2 transition rates for transitions between levels in the $2s^2 2p^2$, $2s2p^3$, and $2p^4$ configurations are shown. Transition rates from this work, $A(RCI)$, are compared for Fe XXI with calculated rates from Landi & Gu (2006), $A(FAC)$, and NIST Atomic Spectra Database (2013), $A(NIST)$. The NIST recommended values are from Shirai et al. (2000). The overall agreement between the present and previous work is good and the average deviation compared to NIST values and FAC calculations amounts to 9.7% and 4.8%, respectively.

Also included in Table 2 is the ratio R of the obtained transition probabilities in length and velocity gauge. For accurate wave functions and strong transitions the ratio R is expected to be close to unity, whereas ratios far from 1 are often associated with weaker transitions where uncertainties normally are larger. On the other hand, ratios close to unity do not necessarily imply accurate wave functions, but together with a thorough validation of calculated level energies these are still strong indicators on the quality of the calculations. As seen in Table 2 the ratios are almost exclusively close to or at unity with only a few exceptions where the transition rates are smaller.

Differences in calculated transition probabilities in length and velocity gauge also reflect the theoretical uncertainty, which must be estimated when experimental observations are lacking. Boron-like O IV, a system for which numerous calculations have been performed, where the scattering in calculated transition rates from different models turns out to be correlated with the ratio R (Rynkun et al. 2012), serves as a good example. In Froese Fischer (2009), the use of the resulting rates in the two gauges as a measure of the theoretical uncertainty is discussed in detail and it is argued that a plausible estimate of the accuracy of LS allowed transition rates, δA, is given by

$$\delta A = (\delta E + \delta S)\, A. \tag{8}$$

In the expression above A is the transition rate computed using the transition energy from observed energy levels ($E_{\rm obs}$), $\delta E = |E_{\rm calc} - E_{\rm obs}|/E_{\rm obs}$ and $\delta S = |S_{\rm length} - S_{\rm velocity}|/\max(S_{\rm length}, S_{\rm velocity})$ where $S_{\rm length}$ and $S_{\rm velocity}$ is the line strength using length and velocity gauge, respectively. Following this method, an average uncertainty of 2.4% is obtained for all transitions between levels in the lower structure. It should be noted that this value probably represents an overestimate since it includes contributions from LS-forbidden transitions for which a comparison of length and velocity values is no longer reliable (Froese Fischer 2009). Based on the above analysis we expect that the calculated transition rates in this work have the better accuracy compared to values from FAC calculations and NIST recommended values, although in a more thorough analysis the transition rates calculated by Landi & Gu (2006) should be corrected with observed transition energies.

In Fig. 2 a synthetic Fe XXI spectrum obtained from calculated transition rates is shown. The intensity of each transition in the spectrum is represented by a Gaussian distribution with a full width at half maximum (FWMH) of 0.05 Å, corresponding to a temperature $T = 10^7$ K, a typical solar flare temperature (Del Zanna et al. 2013). The intensity is set in proportion to $g_j A_{ij} \exp(-E_i/kT)$, where g_j is the statistical weight for the upper level, A_{ij} the transition rate in s^{-1} between the upper level j and the lower i and E_i the excitation energy of the upper level. This scenario corresponds to a high temperature condition where the level population is dominated by collisions. For a low density environment the deexcitation is dominated by the spontaneous decay, and the intensity of each line depends on the excitation rate and the branching fraction. Prominent transitions in the spectrum are

- $2s^2 2p^2\ ^1D_2 - 2s2p^3\ ^1P^\circ_1$ (98.35 Å),
- $2s^2 2p^2\ ^3P_2 - 2s2p^3\ ^3S^\circ_1$ (102.19 Å),
- $2s^2 2p^2\ ^1D_2 - 2s2p^3\ ^1D^\circ_2$ (113.26 Å), and
- $2s2p^3\ ^1P_1 - -2p^4\ ^1S^\circ_0$ (127.08 Å).

The strongest resonance transition in the spectrum is $2s^2 2p^2\ ^3P_0 - 2s2p^3\ ^3D^\circ_1$ (128.75 Å).

6. Conclusions

Self-consistent MCDHF and subsequent RCI calculations have been performed in selected carbon-like ions from Ar XIII to Zn XXV using the GRASP2K program suite. Level energies, Landé g_J-factors, transition energies and transition rates involving the $2s^2 2p^2$, $2s2p^3$, $2p^4$, $2s^2 2p3l$, $2s2p^2 3l$, $2p^3 3l$ and $2s^2 2p4l$ ($l = 0, 1, 2$) configurations have been deduced. To facilitate labeling of states, a transformation from jj-coupling to

LS-coupling to obtain *LS*-precentage compositions has been used. Even so a number of states with identical configuration and leading *LS*-composition are found. Previous theoretical and experimental data for Fe XXI were used to validate computational methods. The energy results from RCI calculations are in excellent agreement with observations. For the $2s^22p^2$, $2p^4$ and $2s2p^3$ configurations, the mean relative energy differences are 0.028% (NIST Atomic Spectra Database 2013) – 0.032% (Landi et al. 2012) whereas, for all other configurations, they are 0.050% (Landi et al. 2012). The uncertainties in transition rates between the lower states have been estimated from the expressions suggested by Froese Fischer (2009) giving an average of only 2.4%. We thus argue that the transition rates are highly accurate and may serve as benchmark for other calculations. The average difference in transition rates from the present calculations and the calculations by Landi & Gu (2006) is 4.8%.

To summarize, the present work has significantly increased the amount of available data for ions in the carbon-like sequence and the resulting level energies and transition rates represent an improvement in accuracy compared with observations as well as with RMBPT calculations by Gu (2005a). A reanalysis of electron temperature and density in solar or astrophysical plasma using the current extended data set allows for a more thorough consistency check with the possibility to identify and include new lines of diagnostic value. In addition, the high accuracy of the current data may rule out the possibility that wrongly identified lines enter the analysis. In the case of Landé g_J-factors the complete data set fills a gap and there is no longer any need to use values derived in the *LS*-coupling scheme that are of limited accuracy for the more ionized ions.

References

Aggarwal, K. M., & Keenan, F. P. 2001, ApJ, 136, 763
Aggarwal, K. M., Keenan, F. P., & Msezane, A. Z. 2003, A&A, 401, 377
Aggarwal, K. M., Keenan, F. P., & Nakazaki, S. 2005, A&A, 436, 1141
Andersson, M., & Jönsson, P. 2008, Comput. Phys. Commun., 178, 156
Badnell, N. R. 1986, J. Phys. B., 19, 3827
Badnell, N. R. 1997, J. Phys. B., 30, 1
Brown, G. V., Beiersdorfer, P., Liedahl, D. A., et al. 2002, ApJS, 140, 589
Chen, M. H., Reed, K. J., McWilliams, D. M., et al. 1997, Atom. Data Nucl. Data Tables, 65, 289
Costa, A. M., Martins, M. C., & Parente, F. 2001, Atom. Data Nucl. Data Tables, 79, 223
Cowan, R. 1981, The theory of atomic structure and spectra (Berkeley: University of California Press)
Del Zanna, G., & Woods, T. N. 2013, A&A, 555, A12
Dyall, K. G., Grant, I. P., Johnson, C. T., Parpia, F. A., & Plummer, E. P. 1989, Comput. Phys. Commun., 55, 425
Eissner, W., Jones, M., & Nussbaumer, H. 1974, Comput. Phys. Commun., 8, 270
Feldman, U., & Doschek, G. A. 2007, Atom. Data Nucl. Data Tables, 93, 779
Feldman, U., Curdt, W., Landi, E., & Wilhelm, K. 2000, ApJ, 544, 508
Froese Fischer, C., & Jönsson, P. 2001, J. Mol. Struct., 537, 55
Froese Fischer, C. 2009, Phys. Scr. T, 134, 014019
Gaigalas, G., Fritzsche, S., & Grant, I. P. 2001, Comput. Phys. Commun., 139, 263
Grant, I. P. 1974, J. Phys. B, 7, 1458
Grant, I. P. 2007, Relativistic Quantum Theory of Atoms and Molecules (New York: Springer)
Gu, M. F. 2005a, ApJS, 156, 105
Gu, M. F. 2005b, Atom. Data Nucl. Data Tables, 89, 267
Gu, M. F. 2007, ApJS, 169, 154
Hu, F., Yang, J., Jiang, G., Wang, C.K., & Zhao, X. F. 2011a, Phys. Scr. T144, 014006
Hu, F., Jiang, G., Yang, J. M., Zhang, J. Y., & Zhao, X. F. 2011b, Acta Physica Polonica A, 120, 429
Jönsson, P., & Froese Fischer, C. 1998 Phys. Rev. A, 57, 4967
Jönsson, P., He, X., Froese Fischer, C., & Grant, I. P. 2007, Comput. Phys. Commun., 177, 597
Jönsson, P., Rynkun, P., & Gaigalas, G. 2011, Atom. Data Nucl. Data Tables, 97, 648
Jönsson, P., Gaigalas, G., Bieroń, J., Froese Fischer, C., & Grant, I. P. 2013a, Comput. Phys. Commun., 184, 2197
Jönsson, P., Ekman, J., Gustafsson, S., et al. 2013b, A&A, 559, A100
Kramida, A., Ralchenko, Yu., Reader, J., & and NIST ASD Team 2012 NIST Atomic Spectra Database (ver. 5.0), National Institute of Standards and Technology, Gaithersburg, MD, http://physics.nist.gov/asd [2013, March 10]
Landi, E., Del Zanna, G., Young, P. R., Dere, K. P., & Mason, H. E. 2012, ApJS, 744, 99
Landi, E., & Gu, M. F. 2006, ApJ, 640, 1171
Landi, E., & Phillips, K. J. H. 2005, ApJS, 160, 286
Liu, H., Jiang, G., Hu, F., Wang, C.-K., Wang, Z.-B., & Yang, J.-M. 2013, Chin. Phys. B, 22, 073202
Martin, W. C., Fuhr, J. R., Kelleher, D. E., et al. 1999, NIST Atomic Spectra Database (ver. 2.0), National Institute of Standards and Technology, Gaithersburg, MD
McKenzie, B. J., Grant, I. P., & Norrington, P. H. 1980, Comput. Phys. Commun., 21, 233
Mason, H. E., Doschek, G. A., Feldman, U., & Bhatia, A. K. 1979, A&A, 73, 74
Olsen, J., Godefroid, M., Jönsson, P., Malmqvist, P. Å., & Froese Fischer, C., 1995, Phys. Rev. E, 52, 4499
Palmeri, P., Quinet, P., Mendoza, C., et al. 2008, ApJS, 177, 408
Petit, V. 2011, Active OB stars: structure, evolution, mass loss, and critical limits, Proc. IAU Symp., 272, 106
Rynkun, P., Jönsson, P., Gaigalas, G., & Froese Fischer, C. 2012, Atom. Data Nucl. Data Tables, 98, 481
Safronova, U. I., & Shlyaptseva, A. S. 1999, Phys. Scr., 60, 36
Shirai, T., Sugar, J., Musgrove, A., & Wiese, W. L. 2000, Spectral Data for Highly Ionized Atoms, Monograph No. 8 (AIP)
Sugar, J., & Corliss, C., 1985, J. Phys. Chem. Ref. Data, 14, 1

Table 1. Energies in cm^{-1} for levels in Fe XXI.

No.	Configuration	LS_J	$E(RCI)$	$E(RCI2)$	$E(RMBPT)$	$E(FAC)$	$E(NIST)$	$E(CHI)$
1	2s(2).2p(2)3P2	$^3P_0$	0	0	0	0	0	0
2	2s(2).2p(2)3P2	$^3P_1$	73 864	73 820	73 867	73 041	73 851	73 851
3	2s(2).2p(2)3P2	$^3P_2$	117 417	117 364	117 372	117 146	117 354	117 367
4	2s(2).2p(2)1D2	$^1D_2$	244 751	244 667	244 581	245 710	244 561	244 568
5	2s(2).2p(2)1S0	$^1S_0$	372 137	372 052	372 261	373 060	371 980	371 744
6	2s_2S.2p(3)4S3	$^5S_2$	486 584	486 521	487 683	479 658	486 950	486 991
7	2s_2S.2p(3)2D3	$^3D_1$	776 775	776 751	777 005	779 724	776 690	776 685
8	2s_2S.2p(3)2D3	$^3D_2$	777 404	777 371	777 655	779 963	777 340	777 367
9	2s_2S.2p(3)2D3	$^3D_3$	803 618	803 562	803 869	805 768	803 540	803 553
10	2s_2S.2p(3)2P1	$^3P_0$	916 444	916 402	916 773	920 272	916 330	916 333
11	2s_2S.12p(3)2P1	$^3P_1$	925 074	925 024	925 408	928 822	924 920	924 920
12	2s_2S.2p(3)2P1	$^3P_2$	942 621	942 556	942 986	946 135	942 430	942 364
13	2s_2S.2p(3)4S3	$^3S_1$	1 096 019	1 096 012	1 095 820	1 105 578	1 095 670	1 095 679
14	2s_2S.2p(3)2D3	$^1D_2$	1 127 672	1 127 631	1 127 460	1 137 533	1 127 240	1 127 250
15	2s_2S.2p(3)2P1	$^1P_1$	1 261 577	1 261 529	1 261 240	1 272 627	1 261 140	1 260 902
16	2p(4)3P2	$^3P_2$	1 646 437	1 646 462	1 646 467	1 657 411	1 646 300	1 646 409
17	2p(4)3P2	$^3P_0$	1 735 823	1 735 831	1 735 813	1 747 301	1 735 700	1 735 715
18	2p(4)3P2	$^3P_1$	1 740 623	1 740 606	1 740 707	1 750 848	1 740 500	1 740 453
19	2p(4)1D2	$^1D_2$	1 817 786	1 817 776	1 817 362	1 832 102	1 817 100	1 817 041
20	2p(4)1S0	$^1S_0$	2 048 512	2 048 489	2 047 850	2 066 463	2 048 200	2 048 056
21	2s(2).2p_2P.3s	$^3P_0$	7 663 283		7 664 054	7 654 119		
22	2s(2).2p_2P.3s	$^3P_1$	7 671 971		7 672 703	7 663 398		7 661 883
23	2s(2).2p_2P.3s	$^3P_2$	7 780 298		7 781 147	7 770 895		
24	2s(2).2p_2P.3s	$^1P_1$	7 803 764		7 804 419	7 796 397		
25	2s(2).2p_2P.3p	$^3D_1$	7 841 903		7 842 922	7 834 847		
26	2s(2).2p_2P.3p: 1	$^3P_1$	7 898 154		7 898 974	7 891 978		
27	2s(2).2p_2P.3p	$^3D_2$	7 901 553		7 902 378	7 895 497		
28	2s(2).2p_2P.3p	$^3P_0$	7 914 849		7 915 811	7 909 434		7 915 463
29	2s(2).2p_2P.3p: 2	$^3P_1$	7 983 446		7 984 350	7 977 011		
30	2s(2).2p_2P.3p	$^3D_3$	7 994 588		7 995 388	7 987 318		
31	2s(2).2p_2P.3p	$^3S_1$	8 004 987		8 005 793	7 998 341		
32	2s(2).2p_2P.3p	$^3P_2$	8 007 326		8 008 319	8 002 052		
33	2s(2).2p_2P.3p	$^1D_2$	8 068 537		8 069 071	8 065 382		
34	2s(2).2p_2P.3d	$^3F_2$	8 078 540		8 079 119	8 072 911		8 074 160
35	2s_2S.2p(2)3P2_4P.3s	$^5P_1$	8 080 551		8 082 001	8 070 805		
36	2s(2).2p_2P.3d	$^3F_3$	8 116 048		8 116 480	8 111 336	8 101 400	8 118 008
37	2s(2).2p_2P.3d: 1	$^3P_2$	8 121 922		8 122 529	8 118 025		8 124 085
38	2s(2).2p_2P.3p	$^1S_0$	8 128 645		8 129 396	8 126 192		8 143 710
39	2s_2S.2p(2)3P2_4P.3s	$^5P_2$	8 131 973		8 133 460	8 121 258		
40	2s(2).2p_2P.3d	$^3D_1$	8 139 290		8 140 735	8 135 992	8 140 000	8 141 785
41	2s_2S.2p(2)3P2_4P.3s	$^5P_3$	8 181 331		8 182 599	8 170 876		
42	2s_2S.2p(2)3P2_4P.3s	$^3P_0$	8 182 172		8 182 844	8 179 292		8 180 254
43	2s(2).2p_2P.3d	$^3F_4$	8 202 073		8 202 670	8 195 771		
44	2s(2).2p_2P.3d	$^1D_2$	8 208 705		8 209 597	8 204 329		
45	2s_2S.2p(2)3P2_4P.3s	$^3P_1$	8 222 156		8 222 948	8 217 390		
46	2s(2).2p_2P.3d	$^3D_3$	8 230 918		8 231 868	8 227 144	(8 195 000)	8 229 642
47	2s(2).2p_2P.3d: 2	$^3P_2$	8 245 453		8 246 428	8 241 436	8 230 900	8 229 642
48	2s(2).2p_2P.3d	$^3P_1$	8 245 737		8 247 075	8 241 557		
49	2s(2).2p_2P.3d	$^3P_0$	8 247 732		8 249 164	8 243 033		
50	2s_2S.2p(2)3P2_4P.3p	$^5D_0$	8 267 963		8 269 220	8 259 742		
51	2s_2S.2p(2)3P2_4P.3p	$^5D_1$	8 270 558		8 272 088	8 262 373		
52	2s_2S.2p(2)3P2_4P.3s	$^3P_2$	8 274 704		8 275 427	8 270 235		
53	2s(2).2p_2P.3d	$^1F_3$	8 300 618		8 301 128	8 301 379	8 313 600	
54	2s(2).2p_2P.3d	$^1P_1$	8 303 730		8 307 428	8 305 376	8 293 900	8 293 791
55	2s_2S.2p(2)3P2_4P.3p	$^5D_2$	8 305 917		8 309 162	8 297 457		
56	2s_2S.2p(2)3P2_4P.3p	$^3S_1$	8 312 499		8 309 359	8 300 070		
57	2s_2S.2p(2)3P2_4P.3p	$^5P_1$	8 349 456		8 350 857	8 342 324		8 350 731
58	2s_2S.2p(2)3P2_4P.3p	$^5D_3$	8 351 775		8 353 277	8 342 522		
59	2s_2S.2p(2)3P2_4P.3p	$^5P_2$	8 352 117		8 353 731	8 343 801		

Notes. $E(RCI)$ this work, $E(RCI2)$ previous RCI calculations by Jönsson et al. (2011), $E(RMBPT)$ relativistic many-body pertubation calculations by Gu (2005a), $E(FAC)$ calculations using the Flexible Atomic Code (FAC) by Landi & Gu (2006), $E(NIST)$ NIST recommended values (NIST Atomic Spectra Database 2013) and $E(CHI)$ observed energies from the Chianti database (Landi et al. 2012). Indices ": 1" and ": 2" are used to differ between identical configurations which share the same coupling and leading LS-percentage composition.

Table 1. continued.

No.	Configuration	LS_J	$E(RCI)$	$E(RCI2)$	$E(RMBPT)$	$E(FAC)$	$E(NIST)$	$E(CHI)$
60	2s_2S.2p(2)3P2_4P.3p	$^3D_1$	8 379 967		8 380 890	8 373 689		8 376 741
61	2s_2S.2p(2)3P2_4P.3p	$^5P_3$	8 388 634		8 390 292	8 380 281		
62	2s_2S.2p(2)3P2_4P.3p	$^5D_4$	8 399 557		8 401 039	8 390 478		
63	2s_2S.2p(2)3P2_4P.3p	$^3D_2$	8 410 077		8 411 182	8 404 386		
64	2s_2S.2p(2)1D2_2D.3s	$^3D_1$	8 420 588		8 421 426	8 420 569		
65	2s_2S.2p(2)1D2_2D.3s	$^3D_2$	8 428 405		8 429 248	8 428 172		
66	2s_2S.2p(2)1D2_2D.3s	$^3D_3$	8 440 926		8 441 758	8 437 725		
67	2s_2S.2p(2)3P2_4P.3p	$^3P_0$	8 442 813		8 443 776	8 438 241		
68	2s_2S.2p(2)3P2_4P.3p	$^5S_2$	8 443 646		8 445 037	8 440 027		
69	2s_2S.2p(2)3P2_4P.3p	$^3D_3$	8 462 365		8 463 510	8 456 502		
70	2s_2S.2p(2)3P2_4P.3p	$^3P_1$	8 467 690		8 468 680	8 462 413		
71	2s_2S.2p(2)3P2_4P.3p	$^3P_2$	8 470 871		8 471 913	8 466 158		
72	2s_2S.2p(2)3P2_4P.3d	$^5F_1$	8 480 620		8 481 735	8 471 575		
73	2s_2S.2p(2)3P2_4P.3d	$^5F_2$	8 488 782		8 489 971	8 479 898		8 486 331
74	2s_2S.2p(2)1D2_2D.3s	$^1D_2$	8 496 990		8 497 512	8 498 660		
75	2s_2S.2p(2)3P2_4P.3d: 1	$^5F_3$	8 506 111		8 507 343	8 497 311		8 511 385
76	2s_2S.2p(2)3P2_4P.3d	$^5F_4$	8 544 575		8 545 928	8 534 831		
77	2s_2S.2p(2)3P2_2P.3s	$^3P_1$	8 545 485		8 546 507	8 544 603		
78	2s_2S.2p(2)3P2_2P.3s	$^3P_0$	8 553 885		8 554 716	8 545 420		
79	2s_2S.2p(2)3P2_4P.3d	$^5D_0$	8 554 798		8 555 918	8 546 365		
80	2s_2S.2p(2)3P2_4P.3d	$^5D_1$	8 555 297		8 556 534	8 547 553		
81	2s_2S.2p(2)3P2_4P.3d	$^5D_2$	8 555 491		8 556 850	8 558 611		
82	2s_2S.2p(2)3P2_4P.3d: 2	$^5F_3$	8 561 662		8 562 969	8 552 789		8 564 535
83	2s_2S.2p(2)3P2_4P.3d	$^3P_2$	8 581 274		8 582 755	8 576 965		8 575 780
84	2s_2S.2p(2)3P2_4P.3d	$^5F_5$	8 586 636		8 588 014	8 577 151		
85	2s_2S.2p(2)3P2_4P.3d	$^5D_4$	8 597 735		8 599 106	8 588 388		
86	2s_2S.2p(2)1D2_2D.3p	$^3F_2$	8 606 110		8 606 654	8 607 148		8 605 427
87	2s_2S.2p(2)3P2_4P.3d	$^3F_2$	8 611 432		8 611 843	8 608 283		
88	2s_2S.2p(2)3P2_4P.3d	$^5P_3$	8 619 312		8 620 847	8 611 148		
89	2s_2S.2p(2)3P2_4P.3d	$^3P_1$	8 632 848		8 634 110	8 624 940		
90	2s_2S.2p(2)3P2_4P.3d	$^5P_2$	8 632 999		8 634 772	8 627 264		
91	2s_2S.2p(2)1D2_2D.3p	$^3F_3$	8 638 806		8 639 402	8 631 484		
92	2s_2S.2p(2)3P2_4P.3d	$^5P_1$	8 639 310		8 641 331	8 638 556		
93	2s_2S.2p(2)3P2_4P.3d	$^3F_3$	8 642 246		8 642 997	8 640 596		
94	2s_2S.2p(2)1D2_2D.3p	$^3D_1$	8 643 164		8 643 819	8 646 413		
95	2s_2S.2p(2)1D2_2D.3p	$^1D_2$	8 652 079		8 652 729	8 654 122		
96	2s_2S.2p(2)1S0_2S.3s	$^3S_1$	8 663 369		8 664 211	8 659 197		
97	2s_2S.2p(2)1D2_2D.3p	$^3F_4$	8 663 995		8 664 698	8 664 020		
98	2s_2S.2p(2)3P2_4P.3d	$^3P_0$	8 664 775		8 665 901	8 664 971		
99	2s_2S.2p(2)1D2_2D.3p	$^3D_2$	8 669 654		8 670 271	8 672 736		
100	2s_2S.2p(2)1D2_2D.3p	$^1F_3$	8 670 238		8 670 921	8 672 774		
101	2s_2S.2p(2)3P2_2P.3s	$^3P_2$	8 678 997		8 679 792	8 684 415		
102	2s_2S.2p(2)1D2_2D.3p	$^3D_3$	8 685 508		8 686 110	8 686 672		
103	2s_2S.2p(2)1D2_2D.3p	$^1P_1$	8 685 523		8 686 131	8 688 610		
104	2s_2S.2p(2)3P2_4P.3d	$^3F_4$	8 690 038		8 691 035	8 688 710		
105	2s_2S.2p(2)1D2_2D.3p	$^3P_0$	8 692 158		8 692 888	8 696 102		
106	2s_2S.2p(2)3P2_2P.3s	$^1P_1$	8 694 748		8 695 448	8 701 378		
107	2s_2S.2p(2)1S0_2S.3s	$^1S_0$	8 705 045		8 705 638	8 705 163		
108	2s_2S.2p(2)1D2_2D.3p	$^3P_1$	8 705 336		8 705 907	8 708 601		
109	2s_2S.2p(2)3P2_4P.3d	$^3D_1$	8 714 259		8 714 891	8 711 939		
110	2s_2S.2p(2)3P2_4P.3d	$^3D_2$	8 718 488		8 719 284	8 716 830		
111	2s_2S.2p(2)3P2_4P.3d	$^3D_3$	8 725 014		8 726 150	8 723 610		
112	2s_2S.2p(2)1D2_2D.3p	$^3P_2$	8 725 573		8 726 160	8 728 210		
113	2s_2S.2p(2)3P2_2P.3p: 1	$^3P_0$	8 728 201		8 729 097	8 733 912		
114	2s_2S.2p(2)3P2_2P.3p	$^3D_1$	8 756 568		8 757 564	8 762 768		
115	2s_2S.2p(2)3P2_2P.3p	$^3D_2$	8 777 614		8 778 384	8 783 967		
116	2s_2S.2p(2)3P2_2P.3p	$^3P_1$	8 783 041		8 783 833	8 788 773		
117	2s_2S.2p(2)1D2_2D.3d	$^3G_3$	8 832 111		8 832 017	8 834 209		
118	2s_2S.2p(2)1D2_2D.3d	$^3G_4$	8 844 277		8 844 450	8 846 181		
119	2s_2S.2p(2)3P2_2P.3p	$^1S_0$	8 849 765		8 850 725	8 853 967		
120	2s_2S.2p(2)1D2_2D.3d	$^3F_2$	8 854 340		8 854 613	8 859 499		
121	2s_2S.2p(2)1D2_2D.3d	$^3G_5$	8 860 935		8 861 284	8 861 717		
122	2s_2S.2p(2)1D2_2D.3d	$^3F_3$	8 861 653		8 861 961	8 866 368		
123	2s_2S.2p(2)1D2_2D.3d	$^3D_1$	8 867 340		8 868 074	8 868 505		

Table 1. continued.

No.	Configuration	LS_J	$E(RCI)$	$E(RCI2)$	$E(RMBPT)$	$E(FAC)$	$E(NIST)$	$E(CHI)$
124	2s_2S.2p(2)1D2_2D.3d	$^3F_4$	8 870 509		8 870 881	8 874 759		
125	2s_2S.2p(2)1D2_2D.3d	$^3D_2$	8 874 519		8 875 243	8 875 571		
126	2s_2S.2p(2)1S0_2S.3p	$^1P_1$	8 875 791		8 876 936	8 879 570		
127	2s_2S.2p(2)1D2_2D.3d	$^3D_3$	8 881 012		8 881 744	8 882 290		
128	2s_2S.2p(2)3P2_2P.3p	$^3D_3$	8 883 090		8 883 727	8 887 411		
129	2s_2S.2p(2)1S0_2S.3p	$^3P_2$	8 884 371		8 885 290	8 890 659		
130	2s_2S.2p(2)3P2_2P.3p	$^3S_1$	8 888 846		8 890 045	8 896 515		
131	2s_2S.2p(2)3P2_2P.3p	$^3P_2$	8 892 966		8 893 680	8 902 114		
132	2s_2S.2p(2)3P2_2P.3p: 2	$^3P_0$	8 896 523		8 897 266	8 902 518		
133	2s_2S.2p(2)1D2_2D.3d	$^1F_3$	8 903 035		8 903 384	8 905 859		
134	2s_2S.2p(2)1D2_2D.3d	$^3P_0$	8 903 428		8 904 177	8 908 798		
135	2s_2S.2p(2)1S0_2S.3p	$^3P_1$	8 905 733		8 906 288	8 909 327		
136	2s_2S.2p(2)1D2_2D.3d	$^3P_1$	8 906 644		8 907 399	8 911 686		
137	2s_2S.2p(2)1D2_2D.3d	$^3P_2$	8 911 313		8 912 031	8 916 517		
138	2s_2S.2p(2)1D2_2D.3d	$^1G_4$	8 911 976		8 912 032	8 917 135		
139	2s_2S.2p(2)1D2_2D.3d: 1	$^3S_1$	8 924 212		8 924 801	8 927 900		
140	2s_2S.2p(2)1D2_2D.3d	$^1D_2$	8 944 182		8 944 873	8 949 206		
141	2s_2S.2p(2)1D2_2D.3d: 2	$^3S_1$	8 945 210		8 945 467	8 950 456		
142	2s_2S.2p(2)3P2_2P.3p	$^1D_2$	8 947 674		8 955 676	8 958 083		
143	2p(3)4S3_4S.3s	$^5S_2$	8 964 946		8 958 640	8 967 005		
144	2s_2S.2p(2)3P2_2P.3d	$^3F_2$	8 971 800		8 972 589	8 980 290		8 970 720
145	2s_2S.2p(2)3P2_2P.3d	$^3F_3$	8 978 976		8 979 625	8 986 183		
146	2s_2S.2p(2)1D2_2D.3d	$^1S_0$	8 983 455		8 983 562	8 989 669		
147	2s_2S.2p(2)1D2_2D.3d	$^1P_1$	8 984 222		8 985 020	8 992 861		
148	2s_2S.2p(2)3P2_2P.3p	$^1P_1$	8 992 824		8 993 171	9 005 735		
149	2s_2S.2p(2)3P2_2P.3d: 1	$^3D_2$	8 998 400		8 998 896	9 005 594		9 001 042
150	2p(3)4S3_4S.3s	$^3S_1$	9 059 790		9 059 933	9 070 201		
151	2s_2S.2p(2)3P2_2P.3d	$^3F_4$	9 082 726		9 083 034	9 088 799		
152	2s_2S.2p(2)1S0_2S.3d	$^3D_3$	9 084 860		9 085 475	9 091 534		
153	2s_2S.2p(2)3P2_2P.3d	$^1P_1$	9 093 578		9 094 667	9 099 804		
154	2s_2S.2p(2)1S0_2S.3d	$^3D_2$	9 098 970		9 100 004	9 105 207		
155	2s_2S.2p(2)3P2_2P.3d	$^3D_3$	9 106 721		9 107 207	9 116 145		
156	2s_2S.2p(2)3P2_2P.3d	$^3D_1$	9 114 500		9 115 490	9 122 411		
157	2s_2S.2p(2)3P2_2P.3d	$^3P_2$	9 119 916		9 120 705	9 125 948		
158	2s_2S.2p(2)3P2_2P.3d: 2	$^3D_2$	9 123 741		9 126 280	9 132 939		
159	2p(3)2D3_2D.3s	$^3D_2$	9 129 452		9 130 111	9 140 913		
160	2p(3)2D3_2D.3s	$^3D_1$	9 131 559		9 132 121	9 142 407		
161	2p(3)4S3_4S.3p: 1	$^5P_1$	9 139 236		9 140 248	9 142 862		
162	2s_2S.2p(2)3P2_2P.3d	$^3P_0$	9 139 246		9 142 678	9 151 409		
163	2p(3)4S3_4S.3p: 2	$^5P_1$	9 145 963		9 144 693	9 152 433		
164	2p(3)4S3_4S.3p	$^5P_2$	9 149 147		9 148 530	9 154 894		
165	2p(3)2D3_2D.3s	$^3D_3$	9 154 233		9 154 936	9 165 349		
166	2s_2S.2p(2)3P2_2P.3d	$^1F_3$	9 154 960		9 155 180	9 170 016		
167	2p(3)4S3_4S.3p	$^5P_3$	9 171 074		9 172 411	9 172 614		
168	2p(3)2D3_2D.3s	$^1D_2$	9 184 102		9 184 397	9 197 442		
169	2p(3)4S3_4S.3p	$^3P_1$	9 204 030		9 205 207	9 209 882		
170	2s_2S.2p(2)3P2_2P.3d	$^1D_2$	9 204 219		9 209 861	9 217 674		
171	2p(3)4S3_4S.3p	$^3P_2$	9 224 440		9 219 886	9 233 574		
172	2p(3)4S3_4S.3p	$^3P_0$	9 232 518		9 233 776	9 236 754		
173	2p(3)2D3_2D.3p	$^3D_1$	9 278 326		9 279 141	9 288 413		
174	2p(3)2P1_2P.3s	$^3P_0$	9 293 415		9 294 251	9 304 899		
175	2p(3)2D3_2D.3p	$^3F_2$	9 297 693		9 298 340	9 309 081		
176	2p(3)2P1_2P.3s	$^3P_1$	9 303 498		9 304 333	9 315 304		
177	2p(3)2D3_2D.3p	$^3D_2$	9 319 246		9 319 700	9 330 821		
178	2p(3)2D3_2D.3p	$^3F_3$	9 319 254		9 319 854	9 331 029		
179	2p(3)2D3_2D.3p: 1	$^1F_3$	9 333 708		9 334 269	9 346 442		
180	2p(3)2D3_2D.3p	$^1P_1$	9 337 471		9 338 237	9 348 127		
181	2p(3)2D3_2D.3p: 2	$^1F_3$	9 351 181		9 351 598	9 356 614		
182	2p(3)2P1_2P.3s	$^3P_2$	9 352 457		9 353 583	9 356 750		
183	2p(3)2D3_2D.3p	$^3F_4$	9 355 158		9 355 697	9 356 882		
184	2p(3)4S3_4S.3d	$^5D_3$	9 355 869		9 357 353	9 356 975		
185	2p(3)4S3_4S.3d	$^5D_0$	9 356 071		9 357 396	9 360 729		
186	2p(3)4S3_4S.3d	$^5D_2$	9 356 195		9 357 436	9 363 198		
187	2p(3)4S3_4S.3d	$^5D_1$	9 356 415		9 357 820	9 363 954		

Table 1. continued.

No.	Configuration	LS_J	$E(RCI)$	$E(RCI2)$	$E(RMBPT)$	$E(FAC)$	$E(NIST)$	$E(CHI)$
188	2p(3)4S3_4S.3d	$^5D_4$	9 359 945		9 361 633	9 367 095		
189	2p(3)2P1_2P.3s	$^1P_1$	9 379 329		9 379 836	9 392 002		
190	2p(3)2D3_2D.3p	$^3P_0$	9 394 163		9 394 106	9 411 350		
191	2p(3)4S3_4S.3d	$^3D_2$	9 410 049		9 411 121	9 417 485		
192	2p(3)2D3_2D.3p	$^3P_1$	9 418 717		9 419 066	9 433 409		
193	2p(3)2D3_2D.3p	$^3P_2$	9 422 708		9 422 791	9 440 269		
194	2p(3)4S3_4S.3d	$^3D_3$	9 434 988		9 436 209	9 441 481		
195	2p(3)4S3_4S.3d	$^3D_1$	9 437 060		9 438 131	9 443 398		
196	2p(3)2D3_2D.3p	$^1D_2$	9 461 732		9 461 868	9 479 514		
197	2p(3)2P1_2P.3p	$^3D_1$	9 470 895		9 471 878	9 484 672		
198	2p(3)2D3_2D.3d	$^3F_2$	9 497 550		9 498 115	9 507 519		
199	2p(3)2P1_2P.3p	$^3D_2$	9 506 366		9 506 959	9 518 109		
200	2p(3)2D3_2D.3d	$^3F_3$	9 507 650		9 508 167	9 519 685		
201	2p(3)2P1_2P.3p	$^3S_1$	9 508 148		9 508 851	9 520 796		
202	2p(3)2D3_2D.3d	$^3G_3$	9 513 273		9 513 576	9 525 026		
203	2p(3)2D3_2D.3d	$^3G_4$	9 515 327		9 515 711	9 526 573		
204	2p(3)2D3_2D.3d	$^1S_0$	9 515 887		9 516 467	9 527 127		
205	2p(3)2D3_2D.3d	$^3D_1$	9 531 988		9 532 635	9 543 735		
206	2p(3)2D3_2D.3d	$^3F_4$	9 533 912		9 534 436	9 544 523		
207	2p(3)2D3_2D.3d	$^3G_5$	9 541 912		9 542 243	9 552 779		
208	2p(3)2D3_2D.3d	$^1G_4$	9 542 106		9 542 329	9 554 096		
209	2p(3)2P1_2P.3p	$^1P_1$	9 546 561		9 547 048	9 559 919		
210	2p(3)2P1_2P.3p	$^3P_0$	9 547 870		9 548 695	9 560 721		
211	2p(3)2P1_2P.3p	$^3D_3$	9 548 860		9 549 544	9 565 350		
212	2p(3)2P1_2P.3p	$^3P_1$	9 576 039		9 576 606	9 590 118		
213	2p(3)2D3_2D.3d	$^3D_2$	9 577 779		9 578 557	9 591 580		
214	2p(3)2D3_2D.3d	$^1P_1$	9 580 581		9 581 027	9 593 328		
215	2p(3)2P1_2P.3p	$^3P_2$	9 587 733		9 588 117	9 601 935		
216	2p(3)2D3_2D.3d	$^3D_3$	9 588 298		9 588 716	9 603 784		
217	2p(3)2P1_2P.3p	$^1D_2$	9 593 774		9 593 872	9 608 454		
218	2p(3)2D3_2D.3d	$^3P_0$	9 596 293		9 596 815	9 611 062		
219	2p(3)2D3_2D.3d	$^3P_2$	9 598 161		9 598 622	9 612 881		
220	2p(3)2D3_2D.3d	$^3P_1$	9 601 373		9 601 722	9 614 007		
221	2p(3)2D3_2D.3d	$^1D_2$	9 618 384		9 619 001	9 633 260		
222	2p(3)2D3_2D.3d	$^3S_1$	9 624 366		9 625 059	9 641 011		
223	2p(3)2D3_2D.3d	$^1F_3$	9 646 766		9 646 771	9 665 006		
224	2p(3)2P1_2P.3d	$^3F_2$	9 690 636		9 691 851	9 704 087		
225	2p(3)2P1_2P.3d	$^3F_3$	9 701 916		9 702 517	9 714 718		
226	2p(3)2P1_2P.3p	$^1S_0$	9 718 240		9 717 625	9 736 559		
227	2p(3)2P1_2P.3d: 1	$^3P_2$	9 720 952		9 721 673	9 741 161		
228	2p(3)2P1_2P.3d	$^3F_4$	9 735 480		9 736 111	9 746 771		
229	2p(3)2P1_2P.3d	$^3P_1$	9 740 645		9 742 719	9 754 847		
230	2p(3)2P1_2P.3d	$^3P_0$	9 748 184		9 749 774	9 758 859		
231	2p(3)2P1_2P.3d: 2	$^3P_2$	9 757 890		9 758 107	9 770 963		
232	2p(3)2P1_2P.3d	$^3D_1$	9 765 663		9 766 056	9 781 499		
233	2p(3)2P1_2P.3d	$^3D_3$	9 780 738		9 781 044	9 794 389		
234	2p(3)2P1_2P.3d	$^1F_3$	9 800 368		9 800 742	9 819 206		
235	2p(3)2P1_2P.3d	$^3D_2$	9 800 852		9 801 738	9 819 939		
236	2p(3)2P1_2P.3d	$^1P_1$	9 879 471		9 879 655	9 902 175		
237	2s(2).2p_2P.4s	$^3P_0$	10 368 077			10 362 393		
238	2s(2).2p_2P.4s	$^3P_1$	10 371 121			10 365 585	10 380 000	
239	2s(2).2p_2P.4p	$^3D_1$	10 442 616			10 437 633		
240	2s(2).2p_2P.4p	$^3P_1$	10 466 102			10 460 676		
241	2s(2).2p_2P.4p	$^3D_2$	10 468 322			10 462 978		
242	2s(2).2p_2P.4p	$^3P_0$	10 470 990			10 465 993		
243	2s(2).2p_2P.4s	$^3P_2$	10 485 597			10 479 693		
244	2s(2).2p_2P.4s	$^1P_1$	10 492 966			10 487 317		
245	2s(2).2p_2P.4d	$^3F_2$	10 532 099			10 526 459		
246	2s(2).2p_2P.4d: 1	$^3P_2$	10 548 542			10 542 323	(10 547 000)	10 547 249
247	2s(2).2p_2P.4d	$^3F_3$	10 549 480			10 543 488	10 548 000	10 548 160
248	2s(2).2p_2P.4d	$^3D_1$	10 554 447			10 548 345	10 553 000	10 553 955
249	2s(2).2p_2P.4p	$^1P_1$	10 568 810			10 563 327		
250	2s(2).2p_2P.4p	$^3D_3$	10 574 912			10 569 412	10 664 000	
251	2s(2).2p_2P.4p	$^3P_2$	10 575 111			10 569 433		

Table 1. continued.

No.	Configuration	LS_J	$E(RCI)$	$E(RCI2)$	$E(RMBPT)$	$E(FAC)$	$E(NIST)$	$E(CHI)$
252	2s(2).2p_2P.4p	$^3S_1$	10 578 203			10 572 657		
253	2s(2).2p_2P.4p	$^1D_2$	10 597 862					
254	2s(2).2p_2P.4p	$^1S_0$	10 619 563					
255	2s(2).2p_2P.4d	$^3F_4$	10 652 979					
256	2s(2).2p_2P.4d	$^1D_2$	10 653 631				10 675 000	
257	2s(2).2p_2P.4d	$^3D_3$	10 660 593					
258	2s(2).2p_2P.4d: 2	$^3P_2$	10 666 807					
259	2s(2).2p_2P.4d	$^3P_1$	10 666 946				10 688 000	
260	2s(2).2p_2P.4d	$^3P_0$	10 667 948					
261	2s(2).2p_2P.4d	$^1F_3$	10 683 984				10 681 000	
262	2s(2).2p_2P.4d	$^1P_1$	10 687 400					

Table 2. Transition rates $A(RCI)$ in units of s^{-1} for E1 transitions in Fe XXI for upper levels 6−20.

Upper	Lower	$E(RCI)$	λ (nm)	$A(RCI)$	R	$A(FAC)$	$A(NIST)$
6	2	412 720	24.229488	3.603E+07	0.93	3.418E+07	3.6E+07
6	3	369 167	27.087986	3.275E+07	0.91	3.190E+07	3.5E+07
6	4	241 833	41.350807	1.309E+06	0.85	1.238E+06	
7	1	776 775	12.873736	1.157E+10	1.00	1.167E+10	1.2E+10
7	2	702 911	14.226540	7.598E+08	1.01	8.035E+08	7.9E+08
7	3	659 358	15.166251	8.347E+07	0.95	7.380E+07	7.3E+07
7	4	532 024	18.796122	1.809E+08	0.94	1.797E+08	2.0E+08
7	5	404 638	24.713440	4.071E+07	0.97	4.207E+07	5.5E+07
8	2	703 540	14.213828	9.241E+09	0.99	9.395E+09	1.0E+10
8	3	659 987	15.151805	4.587E+06	0.83	3.220E+06	1.3E+07
8	4	532 653	18.773939	3.824E+07	0.95	3.697E+07	3.8E+07
9	3	686 201	14.572988	6.104E+09	0.99	6.268E+09	6.6E+09
9	4	558 866	17.893346	9.772E+08	0.97	9.501E+08	1.0E+09
10	2	842 580	11.868298	2.200E+10	1.00	2.252E+10	2.41E+10
11	1	925 073	10.809949	4.213E+09	1.00	4.361E+09	4.28E+09
11	2	851 210	11.747982	1.602E+10	1.00	1.608E+10	1.71E+10
11	3	807 657	12.381491	2.680E+09	1.01	2.879E+09	3.2E+09
11	4	680 323	14.698899	2.577E+08	1.02	2.700E+08	3.0E+08
11	5	552 936	18.085257	1.492E+08	0.94	1.490E+08	1.6E+08
12	2	868 757	11.510688	3.815E+08	0.98	4.295E+08	
12	3	825 204	12.118202	2.039E+10	1.00	2.065E+10	2.17E+10
12	4	697 870	14.329300	1.434E+08	1.04	1.616E+08	2.4E+08
13	1	1 096 019	9.123926	9.457E+09	1.00	9.684E+09	9.9E+09
13	2	1 022 155	9.783245	2.532E+10	1.00	2.586E+10	2.64E+10
13	3	978 602	10.218650	6.103E+10	1.00	6.172E+10	6.4E+10
13	4	851 268	11.747171	3.610E+08	0.98	3.134E+08	3.0E+08
13	5	723 882	13.814401	6.512E+08	0.98	6.176E+08	6.9E+08
14	2	1 053 808	9.489392	3.911E+08	1.01	3.827E+08	4.2E+08
14	3	1 010 255	9.898487	8.022E+09	1.00	7.925E+09	8.8E+09
14	4	882 921	11.326038	4.483E+10	1.00	4.565E+10	4.8E+10
15	1	1 261 577	7.926585	2.857E+07	0.98	2.375E+07	
15	2	1 187 713	8.419538	4.910E+09	1.00	4.842E+09	5.3E+09
15	3	1 144 160	8.740030	2.498E+08	0.99	2.470E+08	2.3E+08
15	4	1 016 826	9.834518	6.584E+10	1.00	6.703E+10	7.1E+10
15	5	889 440	11.243027	1.726E+10	1.00	1.741E+10	1.83E+10
16	6	1 159 853	8.621779	1.423E+09	1.02	1.348E+09	1.4E+09
16	7	869 662	11.498720	3.456E+09	1.01	3.418E+09	3.78E+09
16	8	869 033	11.507038	1.335E+10	1.00	1.354E+10	1.47E+10
16	9	842 819	11.864934	2.821E+10	0.99	2.892E+10	3.09E+10
16	11	721 363	13.862635	3.677E+09	1.00	3.703E+09	3.83E+09
16	12	703 815	14.208262	3.626E+09	0.99	3.616E+09	3.67E+09
16	13	550 417	18.168014	6.004E+09	0.99	6.228E+09	6.8E+09
16	14	518 765	19.276536	7.538E+08	0.98	7.473E+08	8.5E+08
16	15	384 859	25.983478	8.411E+07	0.97	8.806E+07	1.1E+08

Notes. Rates are based on computed transition energies and length gauge has been used. R is the ratio between transition rates in length and velocity gauge. The index for the upper and lower states are the ones given in Table 1. For comparison rates from Landi & Gu (2006), ($A(FAC)$), and NIST Atomic Spectra Database (2013), ($A(NIST)$), are included.

Table 2. continued.

Upper	Lower	$E(RCI)$	λ (nm)	$A(RCI)$	R	$A(FAC)$	$A(NIST)$
17	7	959 047	10.427012	3.473E+10	1.00	3.555E+10	3.73E+10
17	11	810 749	12.334272	1.826E+10	0.99	1.866E+10	2.04E+10
17	13	639 803	15.629801	1.733E+10	1.00	1.758E+10	1.93E+10
17	15	474 245	21.086127	9.923E+06	0.84		
18	6	1 254 038	7.974236	2.382E+08	1.03	2.361E+08	2.8E+08
18	7	963 847	10.375088	1.433E+10	1.00	1.471E+10	1.56E+10
18	8	963 218	10.381859	2.123E+10	1.00	2.186E+10	2.27E+10
18	10	824 178	12.133301	4.810E+09	1.00	4.856E+09	5.1E+09
18	11	815 548	12.261682	1.281E+08	1.02	1.074E+08	1.5E+08
18	12	798 001	12.531311	1.598E+10	0.99	1.619E+10	1.77E+10
18	13	644 603	15.513422	1.290E+10	1.00	1.324E+10	1.4E+10
18	14	612 950	16.314528	3.771E+08	0.97	3.487E+08	3.6E+08
18	15	479 045	20.874858	6.389E+08	0.99	6.361E+08	7.4E+08
19	6	1 331 202	7.512005	5.286E+07	1.02	4.679E+07	
19	7	1 041 011	9.606046	4.029E+06	1.21	5.556E+06	
19	8	1 040 382	9.611850	7.874E+08	1.00	7.573E+08	7.2E+08
19	9	1 014 168	9.860292	5.624E+09	1.01	5.435E+09	5.9E+09
19	11	892 712	11.201813	1.242E+09	1.02	1.181E+09	1.3E+09
19	12	875 164	11.426418	2.516E+09	1.01	2.363E+09	2.5E+09
19	13	721 766	13.854888	6.999E+06	1.00	6.809E+06	
19	14	690 114	14.490350	3.181E+10	1.00	3.274E+10	3.56E+10
19	15	556 209	17.978853	4.497E+09	0.99	4.559E+09	5.0E+09
20	7	1 271 736	7.863266	2.329E+08	0.99	2.083E+08	
20	11	1 123 437	8.901249	4.222E+09	1.01	4.034E+09	4.5E+09
20	13	952 492	10.498774	5.110E+09	1.00	5.272E+09	5.8E+09
20	15	786 934	12.707543	7.547E+10	1.00	7.752E+10	8.4E+10